Research Paper

Calculated and Experimental Infrared Spectra of Substituted Naphthoquinones

Neva Agarwala[#], Daniel Ranke[#], Leyla Rohani, Gary Hastings*

Department of Physics and Astronomy, Georgia State University, Atlanta, Georgia 30302, USA.
**Corresponding author, Gary Hastings, Email: ghastings@gsu.edu*

Received 28 April 2019, revised 14 July 2019, accepted 15 July 2019
Publication Date (Web): July15, 2019

Abstract

In recent years there has been interest in incorporating high-potential, halogenated 1,4-naphthoquinones (NQs) into the A_1 binding site in photosystem I (PSI). This interest in part stems from the considerably altered bioenergetics of electron transfer that occur in PSI with such a substitution. FTIR studies of PSI complexes with halogenated NQs incorporated are also being undertaken. With this in mind it is necessary to consider FTIR absorption spectra of these halogenated quinones in solution, and here we present FTIR absorbance spectra for 2-chloro-1,4-naphthoquinone (2ClNQ), 2-bromo-1,4-naphthoquinone (2BrNQ), 2,3-dichloro-1,4-naphthoquinone (Cl_2NQ) and 2,3-dibromo-1,4-naphthoquinone (Br_2NQ) in tetrahydrofuran (THF). The FTIR spectra of the substituted naphthoquinones (NQs) were compared to FTIR spectra of 2-methyl-3-phytyl-1,4-naphthaquinone (phylloquinone (PhQ)) and 2-methyl-naphthoquinone (2MNQ). To aid in the assignment of bands in the experimental spectra, density functional theory (DFT) based vibrational frequency calculations for all the substituted NQs were undertaken. The calculated and experiment spectra agree well. By calculating normal mode potential energy distributions unambiguous, quantitative band assignments were made. The calculated and experimental spectra make several predictions about what might be observed in time resolved FTIR difference spectra obtained using PSI with the different quinones incorporated.

Keywords

Naphthoquinone, Phylloquinone, FTIR, Density functional theory, vibrational frequency calculations

---

[#]These authors contributed equally to this work.

Abbreviations: FTIR, Fourier transform infrared; H-bond, hydrogen bond; NQ, 1,4-naphthoquinone; PSI, photosystem I; PhQ, phylloquinone (2-methyl-3-phytyl-1,4-naphthoqiuinone); PED, potential energy distribution; 2ClNQ, 2-chloro-1,4-naphthoquinone; 2BrNQ, 2-bromo-1,4-naphthoquinone; Cl_2NQ, 2,3-

dichloro-1,4-naphthoquinone; Br_2NQ, 2,3-dibromo-1,4-naphthoquinone; THF, tetrahydrofuran; DFT, density functional theory.

Introduction

The redox properties of quinones allow them to be utilized in a wide range of functions in different biological systems.[1] In photosynthetic reaction centers (RCs), quinones are well known cofactors in electron transport (ET). In type II RCs, which includes photosystem II (PSII) of oxygen evolving organisms and purple, non-sulfur bacteria, quinones function as terminal electron acceptors in the so-called Q_A and Q_B binding sites.[2,3] Even although the Q_A and Q_B binding sites may be occupied by the same quinone (such as plastoquinone in PSII[4]) their functions are quite different, where the Q_A quinone is an intermediary in ET while the Q_B quinone is involved in proton-coupled ET.[5] In type I RCs, which have iron sulfur clusters as terminal electron acceptors, and includes photosystem I (PSI) from plants and algae, quinones function as an intermediary in transferring electrons from A_0 to F_x.[6,17]

In native PSI a phylloquinone (PhQ) molecule occupies the A_1 binding site.[7] PhQ is a di-substituted 1,4-naphthaquinone (NQ) (2-methyl,3-phtyl-NQ) (also known as Vitamin K_1). Menaquinones (MQs) are identical to PhQ except in the degree of saturation of the hydrocarbon tail,[8] and MQs are found in the Q_A binding site in type II purple bacterial reaction centers from *Blastochloris viridis* and *Chloroflexus aurantiacus*.[9] MQs (and PhQ) can also be substituted into the Q_A binding site in purple bacterial reaction centers from *Rhodobacter sphaeroides*.[3] The function of substituted NQs in both type I and II RCs is therefore of some interest.[10] In particular, exactly how the substituent groups of the NQs can alter or modulate their redox properties of quinones in protein binding sites is of considerable interest.[11]

In recent years it has become possible to substitute a range of different NQs into the A_1 binding site in PSI.[3,12] These PSI particles with different NQs incorporated into the A_1 binding site are now being studied using FTIR difference spectroscopy,[13,14] and of particular interest for the purposes of this manuscript is PSI with different halogenated NQs incorporated. The overall goal in FTIR studies of PSI with different NQs incorporated is the identification of bands in the spectra that are associated with the neutral and reduced states of the incorporated NQs. These bands will provide information on pigment protein interactions that may help modulate the redox properties of the incorporated quinones.[4,7,14,15] Study of halogenated NQs in the A_1 binding site is very interesting, not only in terms of the FTIR difference spectra, but also in terms of the bioenergetics, which are very different. Halogenated NQs intrinsically have a very high redox potential, and even in the A_1 binding site in PSI, the $P700^+A_1^-$ radical pair state is considerably lower in energy than the $P700^+F_X^-$ state, making uphill ET from A_1^- to F_X essentially impossible. Therefore, the $P700^+A_1^-$ state decays by radical pair recombination, which occurs on a tens to hundreds of microsecond timescale at both 298 and 77 K.[11,16] This simplifies the collection of highly-sensitive time resolved (TR) FTIR DS.[17]

When considering bands in TR FTIR DS obtained using PSI with different NQs incorporated, the starting point is to first obtain and interpret the FTIR spectrum of the NQ in solution. Such an interpretation invariably involves (more recently) the use of quantum chemical computational methods to simulate the experimental spectra. These suggested initial steps are the subject of this manuscript.

In this manuscript FTIR absorbance spectra for 2-chloro-1,4-naphthoquinone (2ClNQ), 2-bromo-1,4-naphthoquinone (2BrNQ), 2,3-dichloro-1,4-naphthoquinone (Cl_2NQ), and 2,3-dibromo-1,4-naphthoquinone (Br_2NQ) in tetrahydrofuran (THF) are obtained. These spectra are compared to that obtained for PhQ (and DMNQ) and 2MNQ in THF. In addition, in order to help assign bands in the experimental spectra density functional theory (DFT) based vibrational frequency calculations are undertaken.

Materials and Methods

All quinones and solvents used here were obtained from Sigma-Aldrich Inc. (St Louis, MO), and used as received. 2ClNQ was obtained from Pure-Chemistry Scientific (Burlington, MA) and used as received.

FTIR absorption spectra of the NQs were measured using a Varian 600 UMA FTIR microscope (Varian Inc., MA, USA), utilizing a mercury cadmium telluride detector. Spectra were collected at

4 cm^{-1} resolution. The different NQs were dissolved in tetrahydrofuran (THF) at various concentrations, and a small drop (<5 μL) was deposited on a zinc selenide window. An FTIR spectrum of pure THF was obtained and interactively subtracted.

Calculations were undertaken using Gaussian16 software.[18] (Gaussian Inc. Wallingford, CT). The phytyl tail of PhQ was truncated to a 5-carbon unit [$CH_2CHC(CH_3)_2$]. DFT calculations were performed using the B3LYP functional in combination with the 6-31+G(d) basis set[19]. The solvent was considered using the integral equation formalism (IEF) of the polarizable continuum model (PCM),[20] as it is implemented in Gaussian16. Harmonic, normal mode vibrational frequency calculations result in "stick spectra", which we convolve with Gaussian functions of 4 cm^{-1} half-width, to produce more realistic looking calculated spectra.

Assignment of calculated vibrational frequencies to molecular groups is often based on the calculation of potential energy distributions (PEDs) associated with the normal modes. PEDs are calculated using VEDA.[21] PEDs provide an estimate of how much a specific molecular group vibration contributes to a normal mode.

Results and Discussion

Figure 1 shows the structure and numbering for the six quinones considered in this study. PhQ is the same as 2MNQ except that the phytyl chain is replaced with a hydrogen atom. Figure 2 shows FTIR absorption spectra in the 1750-1200 cm^{-1} spectral region for PhQ, 2MNQ, 2ClNQ, 2BrNQ, Cl_2NQ, and Br_2NQ in THF. A spectrum for PhQ cast in a film of hexane has been obtained previously, and is very similar to that presented in Figure 2.[22] A spectrum for 2,3-dimethyl-1,4-naphthaquinone (DMNQ) in CCl_4 has also been obtained.[23] DMNQ is the same as PhQ except the phytyl chain has been replaced with a methyl group, and it is found that the FTIR absorption spectra of PhQ and DMNQ (in the 1680-1580 cm^{-1} region) are nearly identical.

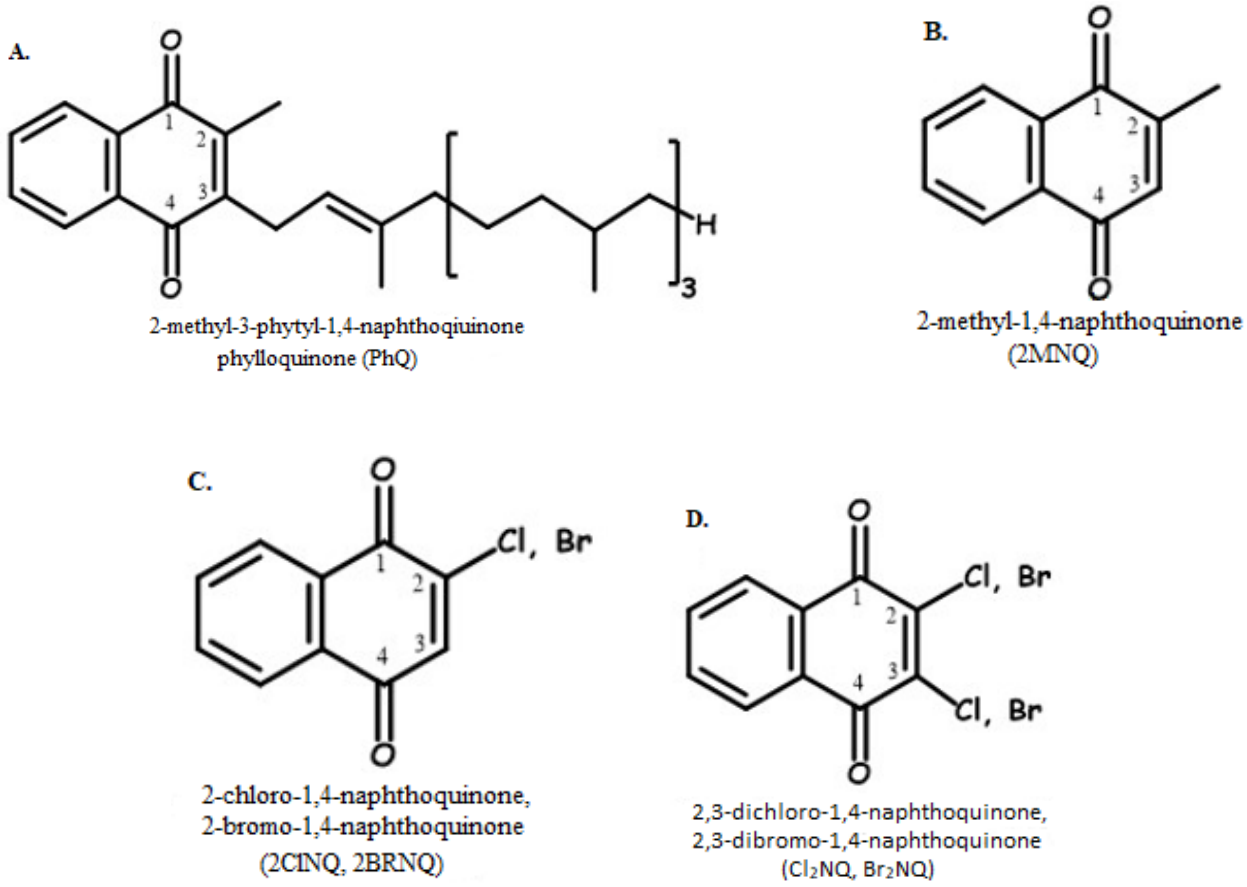

Figure 1: Structure and numbering of the different NQs considered here.

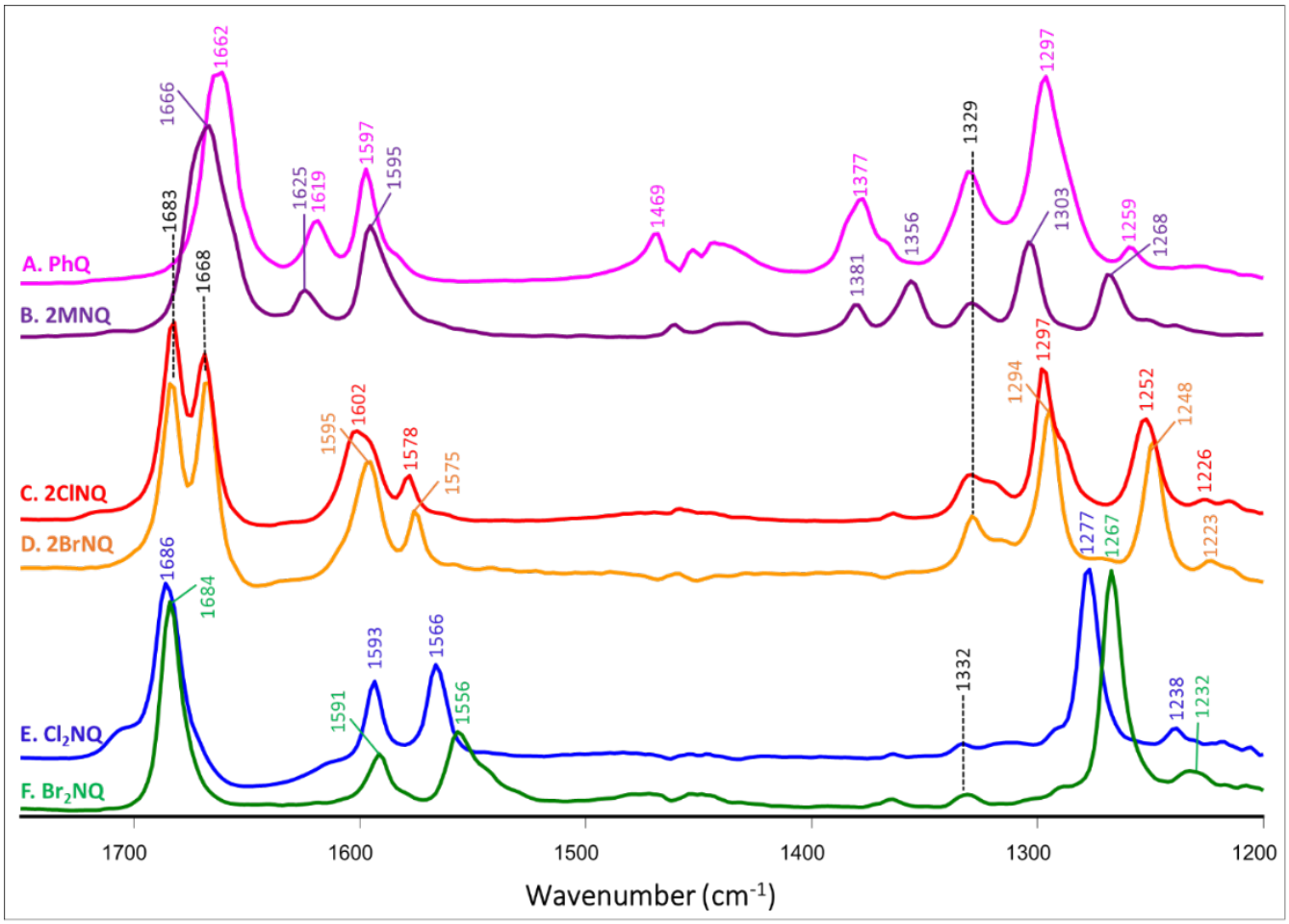

Figure 2: Experimental FTIR absorption spectra for (A) PhQ, (B) 2MNQ, (C) 2ClNQ, (D) 2BrNQ, (E) Cl_2NQ, and (F) Br_2NQ in THF. The spectra were scaled (1695-1640 cm^{-1}) so that the intensities of the bands around 1684 cm^{-1} are similar.

Figure 3 shows DFT calculated FTIR spectra for the six quinones considered in this study. The PEDs associated with the normal modes that give rise to the most intense bands in the spectra in Figure 3 are listed in Table 1. The calculated and experimental spectra clearly display similarities in both peak positions and in relative band intensities. How the calculated and experimental bands are associated is indicated in Table 1. In this manuscript calculated frequencies are scaled by 0.978[24], which is arbitrarily chosen so that the observed band at 1662 cm^{-1} for neutral PhQ matches the frequency for the calculated band.

Modes of the phytyl chain of PhQ.

PhQ in THF (Figure 2A) displays bands at 1469 and 1377 cm^{-1} that are absent in the spectra of the other NQs (Figure 2). These bands are therefore likely to be associated with the hydrocarbon phytyl chain of PhQ. The calculations support this notion, and show that the 1469 cm^{-1} band is due to CH_2 bending modes [$\delta(CH_2)$] of the phytyl-tail, while the 1377 cm^{-1} band is due to both $\delta(CH_2)$ and $\delta(CH_3)$ modes of the phytyl-tail (Table 1). This conclusion also agrees with previous studies.[13,25] These assignments indicate the appropriateness of the computational methods used here.

Quinone C=O vibrations.

For PhQ in THF the most intense absorption band is found at 1662 cm^{-1}, and calculations indicate that this band is due to the antisymmetric stretching vibration of both C=O groups (C_1=O, 54% and C_4=O, 30%)

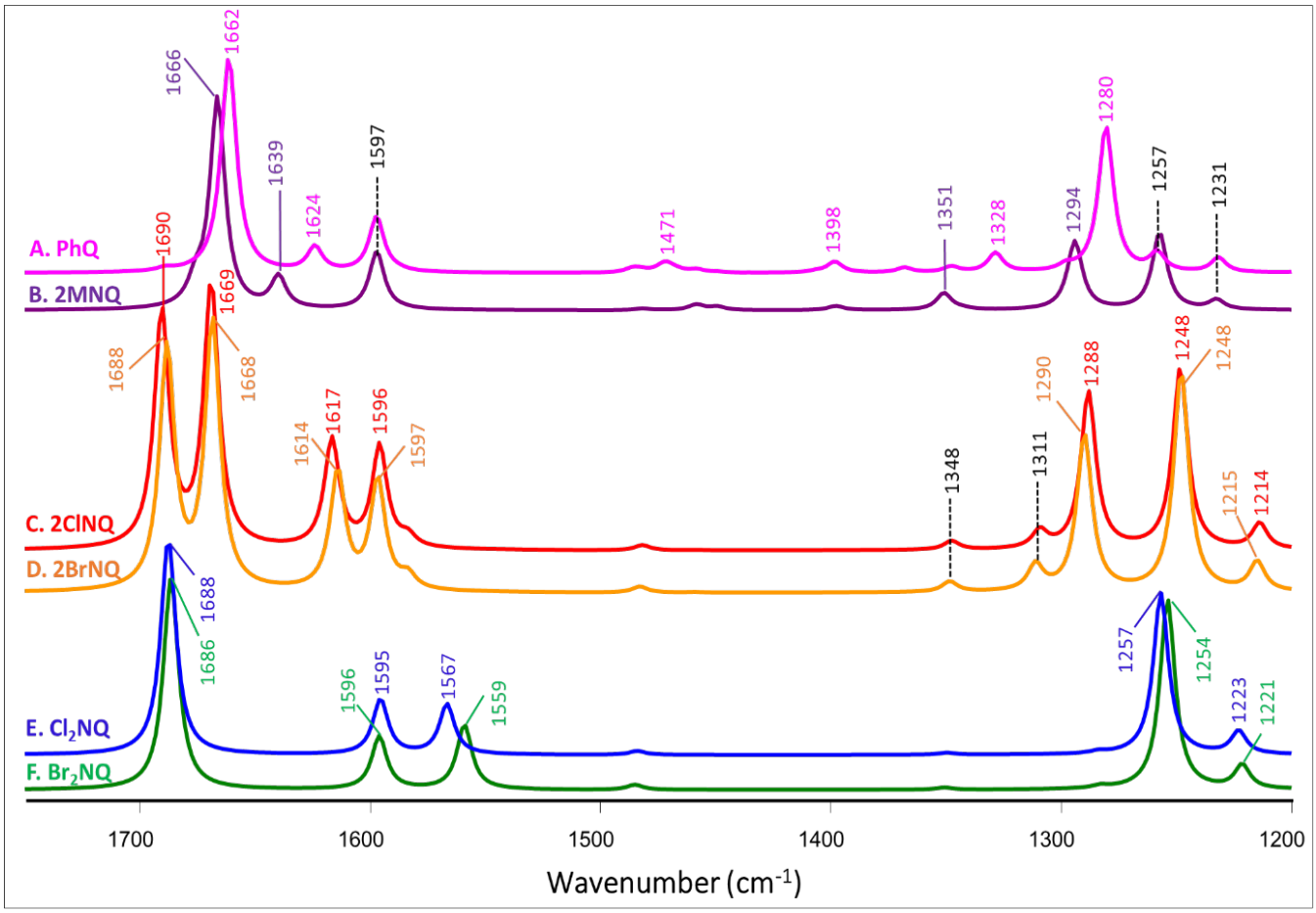

Figure 3: Calculated IR absorption spectra for (A) PhQ, (B) 2MNQ, (C) 2ClNQ, (D) 2BrNQ, (E) Cl_2NQ, and (F) Br_2NQ in THF. Frequencies are scaled by 0.978[24]. Spectra were scaled so that the intensities of the bands between 1688-1662 cm^{-1} are similar. The actual intensities (in km/mol) are indicated in Table 1.

Table 1: Calculated normal mode vibrational frequencies (in cm^{-1}) and intensities (in km/mol) for the six NQs in THF. Only the most intense normal modes are listed. Frequencies are scaled by 0.978 to compare to experimental band frequencies, which are also listed. Potential energy distributions (PED) (in %) are also listed. Only molecular groups with PED above 10% are included. *Abbreviations*: *ν*, bond stretching; *δ*, bending vibration; a, aromatic part of NQ ring; *q,* quinonic part of NQ ring; H*, hydrogen atom attached at position C_3; AS, antisymmetric.

Experimental frequencies (in THF) (cm^{-1})	Calculated frequencies (in THF) (cm^{-1})	Intensity (km/mol)	Potential Energy Distribution (%)
PhQ			
1662	1662	765.7	$[\nu(C_1{=}O)\ 54\% + \nu(C_4{=}O)\ 30\%]_{AS}$
1619	1624	90.8	$\nu(C_2{=}C_3)$ 68%

1597	1597	204.7	ν(C-C)$_a$ 64%
1469	1471	26.7	$\delta(CH_2)_{Methyl\text{-}tail}$ 49% + $\delta(CH_2)_{tail}$ 27%
1377	1398	71.8	$\delta(CH_2)_{tail}$ 85%
1297	1280	540.5	ν(C-C)$_a$ 10% + ν(C-C)$_q$ 39%
2MNQ			
1666	1666	765.9	[$\nu(C_1{=}O)$ 52% + $\nu(C_4{=}O)$32%]$_{AS}$
1625	1639	114.6	$\nu(C_2{=}C_3)$ 68%
1595	1597	210.6	ν(C-C)$_a$ 65%
1356	1351	61.9	ν(C-C)$_a$ 10% + ν(C-C)$_q$ 10%+ δ(CCH*) 17%+ δ(CCH)$_a$ 12%
1303	1294	249.6	ν(C-C)$_q$ 71%
1268	1257	278.9	ν(C-C)$_q$ 16% + δ(CCH)$_a$ 22%
2ClNQ			
1683	1690	403.8	$\nu(C_1{=}O)$ 86%
1668	1669	450.1	$\nu(C_4{=}O)$ 83%
1602	1617	185.6	$\nu(C_2{=}C_3)$ 72%
1578	1596	174.7	ν(C-C)$_a$ 63%
1297	1288	269.7	ν(C-C)$_q$ 32% +δ(CCH)$_q$ 12%+δ(CCH)$_a$ 14%
1252	1248	310.5	ν(C-C)$_q$ 10% +δ(CCH)$_a$ 25%
1226	1214	43.9	ν(C-C)$_q$ 28% +δ(CCH)$_a$ 10% + δ(CCH*) 17%
2BrNQ			
1683	1688	396.5	$\nu(C_1{=}O)$ 85%
1668	1668	437.9	$\nu(C_4{=}O)$ 82%
1595	1614	194.1	$\nu(C_2{=}C_3)$ 71%
1575	1597	180.2	ν(C-C)$_a$ 63%
1329	1311	42.3	ν(C-C)$_q$ 13% +δ(CCC)$_q$ 14%+ δ(CCH*) 36%
1294	1290	257.2	ν(C-C)$_q$ 34%+ δ(CCH)$_a$ 16%
1248	1248	361.2	ν(C-C)$_q$ 11%+ δ(CCH)$_a$ 25%
1223	1215	48.0	ν(C-C)$_q$ 28%+ δ(CCH)$_a$ 26%
Cl_2NQ			
1686	1688	789.8	[$\nu(C_1{=}O)$ 44%+ $\nu(C_4{=}O)$44%]$_{AS}$
1593	1595	153.0	ν(C-C)$_a$ 68%
1566	1567	188.9	$\nu(C_2{=}C_3)$ 73%
1277	1257	607.9	ν(C-C)$_a$ 11% + ν(C-C)$_q$ 42%
1238	1223	86.2	ν(C-C)$_q$ 23% + δ(CCH)$_a$ 27%
Br_2NQ			
1684	1686	755.8	[$\nu(C_1{=}O)$ 44%+ $\nu(C_4{=}O)$45%]$_{AS}$
1591	1596	153.1	ν(C-C)$_a$ 66%
1556	1559	233.1	$\nu(C_2{=}C_3)$ 68%
1267	1254	688.8	ν(C-C)$_q$ 52%
1232	1221	85.2	ν(C-C)$_q$ 25% + δ(CCH)$_a$ 29%

(Table. 1). For 2MNQ in THF a similar intense peak is observed at 1666 cm^{-1} with a weak shoulder near 1670 cm^{-1} (Figure 2B). Computationally the intense 1666 cm^{-1} band is also assigned to an antisymmetric stretching vibration of both C=O groups (C_1=O, 52% and C_4=O, 32%) (Table. 1). Similarly, for Cl_2NQ and Br_2NQ in THF intense bands are observed at 1686 and 1684 cm^{-1}, respectively. This is an upshift of 26 and 22 cm^{-1} relative to the same band of PhQ. Importantly, the observed upshift is very similar to that predicted

computationally (26 and 24 cm^{-1}). In addition, the normal mode giving rise to the intense bands at 1686 and 1684 cm^{-1} for Cl_2NQ and Br_2NQ is again calculated to be an antisymmetric coupled vibration of both the C_1=O and C_4=O groups (For Cl_2NQ: C_1=O, 44% and C_4=O, 44%. For Br_2NQ: C_1=O, 44% and C_4=O, 45%) (Table. 1).

For 2ClNQ and 2BrNQ in THF the main intense peak discussed above is split into two separate peaks at 1683 and 1668 cm^{-1} (Figure 2C, D). Such a clear (15 cm^{-1}) splitting is in agreement with calculations, which indicate intense bands at 1688-1690 and 1668-1669 cm^{-1} (Figure 3C, D). The 1683 and 1668 cm^{-1} bands for 2ClNQ and 2BrNQ in THF are predicted to be due to C_1=O (86%) and C_4=O (83%) vibrations (Table. 1). This is an interesting result, as it is not observed or calculated for 2MNQ, which one might anticipate to have spectra more similar to that of 2ClNQ or 2BrNQ than that for Cl_2NQ or Br_2NQ.

Quinonic and aromatic ring C=C vibrations.

For PhQ in THF an absorption band is observed at 1619 cm^{-1} (Figure 2A). A similar band is calculated at 1624 cm^{-1} (Figure 3A), and is predicted to be mainly due to a C_2=C_3 stretching vibration ($\nu(C_2=C_3)$, 68%) (Table. 1). For 2MNQ in THF the corresponding band is upshifted 6 cm^{-1} compared to PhQ to 1625 cm^{-1} ($\nu(C_2=C_3)$, 68%) (Table. 1). However, the calculated upshift is 15 cm^{-1} (Table 1).

For PhQ in THF an absorption band is observed at 1597 cm^{-1} (Figure 2A). A similar band is calculated at the same frequency (Figure 3A), and is predicted to be mainly due to a C=C stretching associated with the aromatic part of the NQ ring ($\nu(C=C)_a$, 64%) (Table. 1). For 2MNQ in THF the corresponding band is downshifted 2 cm^{-1} compared to PhQ at 1595 cm^{-1} ($\nu(C=C)_a$, 65%) (Table. 1). This agrees with calculations which predict the $\nu(C=C)_a$ mode to be at the same frequency for both 2MNQ and PhQ (Table 1).

For PhQ and 2MNQ the $\nu(C_2=C_3)$ vibration is at a higher frequency than the $\nu(C=C)_a$ vibration. This appears to be true for 2BrNQ and 2ClNQ, although the reverse is calculated to be true for Cl_2NQ and Br_2NQ.

For 2ClNQ and 2BrNQ in THF bands are observed at 1602 and 1595 cm^{-1}, respectively. Corresponding bands appear to be calculated ~15 cm^{-1} higher in frequency at 1617 and 1614 cm^{-1}, however. These bands are due to the $\nu(C_2=C_3)$ vibration. The corresponding bands for Cl_2NQ and Br_2NQ in THF (at least from a visual inspection of the spectra) are observed at 1593 and 1591 cm^{-1}, respectively. Corresponding bands appear to be calculated at very similar frequencies (1595 and 1596 cm^{-1}). These bands are due to the $\nu(C=C)_a$ vibration, however.

For 2ClNQ and 2BrNQ in THF bands are observed at 1578 and 1575 cm^{-1}, respectively (Figure 2). Corresponding bands appear to be calculated at 1596 and 1597 cm^{-1}. These bands are due to the $\nu(C=C)_a$ vibration. The corresponding bands for Cl_2NQ and Br_2NQ in THF (at least from a visual inspection of the spectra) are observed at 1566 and 1556 cm^{-1}, respectively. Corresponding bands appear to be calculated at very similar frequencies (1567 and 1559 cm^{-1}). These bands are due to the $\nu(C_2=C_3)$ vibration, however.

In summary, all of the experimental and calculated spectra show three or four bands in the 1550-1690 cm^{-1} region. The highest frequency bands are due to C_1=O and C_4=O vibrations, or an antisymmetric combination of both. The next two lower intensity bands are due to $\nu(C_2=C_3)$ and $\nu(C=C)_a$ vibrations, with the $\nu(C_2=C_3)$ vibration being higher in frequency than the $\nu(C=C)_a$ vibration for PhQ, 2MNQ, 2ClNQ and 2BrNQ, and lower for Cl_2NQ and Br_2NQ. One noteworthy point is that for Cl_2NQ in THF the FTIR spectrum in Figure 2E displays shoulders on the high frequency sides of some of the above discussed absorption bands. These shoulders are of unknown origin at present. A second noteworthy point is that the relative intensities of the three (or four) bands in the experimental spectra overall agree reasonably well with the calculated spectra.

PhQ in THF displays an intense band at 1297 cm^{-1}, which is at least as intense as the 1662 cm^{-1} band (Figure 2A). Such an intense band is calculated at 1280 cm^{-1}, and is predicted to be due to $\nu(C\text{-}C)_a$ (10%) and $\nu(C\text{-}C)_q$ stretching (39%). Most TR FTIR DS experiments of native PSI have focused on a spectral region above 1400 cm^{-1}. However, the calculated and experimental spectra presented here indicate that extending work to lower frequency (to ~ 1200 cm^{-1}) might be useful for the identification of a band of neutral PhQ in the A_1 binding site. Prior to undertaking this experiment, however, it will off course be useful to calculate spectra for PhQ^- to establish how and if this band is altered upon anion formation.

The PhQ band calculated at 1280 cm^{-1} in Figure 3A is found downshifted ~15 cm^{-1} to 1257-1254 cm^{-1} for Cl_2NQ and Br_2NQ (Figure 3E, F). This calculated result suggests the bands at 1277 and 1267 cm^{-1} in the Cl_2NQ and Br_2NQ FTIR spectra in Figure 2E and F correspond to the 1297 cm^{-1} band for PhQ. This result,

suggesting an intense band of neutral PhQ near 1295 cm^{-1}, and corresponding bands of neutral Cl_2NQ and Br_2NQ ~20-30 cm^{-1} lower in frequency, may be extremely useful and help in the identification of bands in future TR FTIR DS obtained using PSI with neutral Cl_2NQ and Br_2NQ incorporated. The value of this result is even greater when one considers that in the past it has proven very difficult to unambiguously identify absorption bands associated with the neutral quinones incorporated into PSI.

It appears that the calculated band of PhQ at 1280 cm^{-1} is split into two bands for 2ClNQ and 2BrNQ. Such a splitting is also found in the 2MNQ calculated spectra. For 2ClNQ and 2BrNQ bands are found at 1290-1288 and 1248 cm^{-1}. The former band is upshifted ~9 cm^{-1} (relative to the 1280 cm^{-1} band of PhQ) and is due to [$\nu(C\text{-}C)_q$ (32%) + $\delta(CCH)_q$ (12%) + $\delta(CCH)_a$ (14%)]. The latter band is downshifted 32 cm^{-1} and is due to [$\nu(C\text{-}C)_q$, (10%) + $\delta(CCH)_a$ (25%)]. These calculated spectra suggest that the bands at 1290-1288 and 1248 cm^{-1} could correspond to the bands at 1297-1294 and 1252-1248 cm^{-1} in the experimental spectra for 2ClNQ and 2BrNQ in THF. Again, the calculated and experimental spectra presented here predict that bands of neutral 2BrNQ and 2ClNQ may be found at ~1295 and ~1250 cm^{-1} in TR FTIR DS obtained using PSI with 2BrNQ and/or 2ClNQ incorporated into the A_1 binding site. We will certainly be on the lookout for such features in the TR FTIR DS when they become available.

Conclusions

FTIR absorption spectra for six NQs in THF are presented. Corresponding calculated spectra are also presented, and indicate detailed normal mode assignments for the bands in the experimental spectra. For PhQ in THF a band is observed at 1469 cm^{-1}, which is absent in FTIR spectra for the other quinones, indicating that this band is due to vibrations associated with the phytyl tail of PhQ.

Neutral PhQ/2MNQ/Cl_2NQ/Br_2NQ in THF gives rise to an intense absorption band at 1662/1666/1686/1684 cm^{-1}, respectively, that calculations indicate is due to the antisymmetric coupled vibration of both C=O groups. For 2ClNQ/2BrNQ in THF this band is split into two bands, the higher/lower frequency band being due to the C_1=O/C_4=O stretching vibration, respectively.

FTIR spectra of PhQ/Cl_2NQ/Br_2NQ in THF display an intense absorption band at 1297/1277/1267 cm^{-1}, respectively, that calculations indicate is due to a C-C stretching of both the aromatic and quinonic parts of the NQ ring. For 2MNQ/2ClNQ/2BrNQ in THF this band is split into two. The spectra presented here suggest or lead to predictions about the location of quinone bands that may be found in TR FTIR DS.

Acknowledgements

GH acknowledges support from the Department of Energy (DE-SC0017937). GH also acknowledges the use of Georgia State's research computing resources that are supported by Georgia State's Research Solutions. The statements made herein are solely the responsibility of the authors.

References

1 Nohl, H., Jordan, W. & Youngman, R. J. Quinones in Biology: Functions in electron transfer and oxygen activation. Advances in Free Radical Biology & Medicine 2, 211-279, doi: https://doi.org/10.1016/S8755-9668(86)80030-8 (1986).

2 de Wijn, R. & van Gorkom, H. J. Kinetics of Electron Transfer from QA to QB in Photosystem II. Biochemistry 40, 11912-11922, doi:10.1021/bi010852r (2001).

3 Breton, J., Boullais, C., Burie, J. R., Nabedryk, E. & Mioskowski, C. Binding sites of quinones in photosynthetic bacterial reaction centers investigated by light-induced FTIR difference spectroscopy: assignment of the interactions of each carbonyl of QA in Rhodobacter sphaeroides using site-specific 13C-labeled ubiquinone. Biochemistry 33, 14378-14386, doi:10.1021/bi00252a002 (1994).

4 Saito, K., Rutherford, A. W. & Ishikita, H. Mechanism of proton-coupled quinone reduction in Photosystem II. Proceedings of the National Academy of Sciences of the United States of America 110, 954-959, doi:10.1073/pnas.1212957110 (2013).

5 Zhu, Z. & Gunner, M. R. Energetics of Quinone-Dependent Electron and Proton Transfers in Rhodobacter sphaeroides Photosynthetic Reaction

Centers. Biochemistry 44, 82-96, doi:10.1021/bi048348k (2005).
6 Hou, H. J. M. & Mauzerall, D. The A-FX to FA/B Step in Synechocystis 6803 Photosystem I Is Entropy Driven. Journal of the American Chemical Society 128, 1580-1586, doi:10.1021/ja054870y (2006).
7 Shinkarev, V. P., Zybailov, B., Vassiliev, I. R. & Golbeck, J. H. Modeling of the P700+ charge recombination kinetics with phylloquinone and plastoquinone-9 in the A1 site of photosystem I. Biophysical journal 83, 2885-2897 (2002).
8 Beulens, J. W. J. et al. The role of menaquinones (vitamin K2) in human health. British Journal of Nutrition 110, 1357-1368, doi:10.1017/S0007114513001013 (2013).
9 Kishi, S., Saito, K., Kato, Y. & Ishikita, H. Redox potentials of ubiquinone, menaquinone, phylloquinone, and plastoquinone in aqueous solution. Photosynthesis Research 134, 193-200, doi:10.1007/s11120-017-0433-4 (2017).
10 Coates, C. S. et al. The Structure and Function of Quinones in Biological Solar Energy Transduction: A Cyclic Voltammetry, EPR, and Hyperfine Sub-Level Correlation (HYSCORE) Spectroscopy Study of Model Naphthoquinones. The Journal of Physical Chemistry B 117, 7210-7220, doi:10.1021/jp401024p (2013).
11 Mula, S. et al. Incorporation of a high potential quinone reveals that electron transfer in Photosystem I becomes highly asymmetric at low temperature. Photoch Photobio Sci 11, 946-956, doi:10.1039/C2PP05340C (2012).
12 Makita, H. & Hastings, G. Inverted-region electron transfer as a mechanism for enhancing photosynthetic solar energy conversion efficiency. Proceedings of the National Academy of Sciences 114, 9267, doi:10.1073/pnas.1704855114 (2017).
13 Makita, H., Rohani, L., Zhao, N. & Hastings, G. Quinones in the A1 binding site in photosystem I studied using time-resolved FTIR difference spectroscopy. Biochimica et Biophysica Acta (BBA) - Bioenergetics 1858, 804-813, doi:http://dx.doi.org/10.1016/j.bbabio.2017.06.006 (2017).
14 Breton, J. & Nabedryk, E. Protein-quinone interactions in the bacterial photosynthetic reaction center: light-induced FTIR difference spectroscopy of the quinone vibrations. Biochimica et Biophysica Acta (BBA) - Bioenergetics 1275, 84-90, doi:https://doi.org/10.1016/0005-2728(96)00054-0 (1996).
15 Hellwig, P. Infrared spectroscopic markers of quinones in proteins from the respiratory chain. Biochimica et Biophysica Acta (BBA) - Bioenergetics 1847, 126-133, doi:https://doi.org/10.1016/j.bbabio.2014.07.004 (2015).
16 Makita, H. & Hastings, G. Directionality of electron transfer in cyanobacterial photosystem I at 298 and 77K. FEBS Letters 589, 1412-1417, doi:https://doi.org/10.1016/j.febslet.2015.04.048 (2015).
17 Hastings, G. in Photosystem I: The Light Driven Plastocyanin:Ferredoxin Oxidoreductase. Advances in Photosynthesis and Respiration vol 24 (ed JH Golbeck) Ch. 20, 301-318 (Springer, 2006).
18 Gaussian 16 Rev. B.01 (Wallingford, CT, 2016).
19 Bandaranayake, K. M. P., Sivakumar, V., Wang, R. L. & Hastings, G. Modeling the A(1) binding site in photosystem - I. Density functional theory for the calculation of "anion-neutral" FTIR difference spectra of phylloquinone. Vibrational Spectroscopy 42, 78-87, doi:10.1016/j.vibspec.2006.01.003 (2006).
20 Tomasi, J., Cammi, R., Mennucci, B., Cappelli, C. & Corni, S. Molecular properties in solution described with a continuum solvation model. Phys Chem Chem Phys 4, 5697-5712 (2002).
21 Jamróz, M. H. Vibrational energy distribution analysis (VEDA): scopes and limitations. Spectrochimica Acta Part A: Molecular and Biomolecular Spectroscopy 114, 220-230 (2013).
22 Breton, J., Burie, J. R., Berthomieu, C., Berger, G. & Nabedryk, E. The binding sites of quinones in photosynthetic bacterial reaction centers investigated by light-induced FTIR difference spectroscopy: assignment of the QA vibrations in Rhodobacter sphaeroides using 18O- or 13C-labeled ubiquinone and vitamin K1. Biochemistry 33, 4953-4965 (1994).
23 Breton, J., Burie, J.-R., Boullais, C., Berger, G. & Nabedryk, E. Binding sites of quinones in photosynthetic bacterial reaction centers investigated by light-induced FTIR difference spectroscopy: Binding of chainless symmetrical quinones to the QA site of Rhodobacter sphaeroides. Biochemistry 33, 12405-12415, doi:10.1021/bi00207a007 (1994).

24 Frisch, J. B. F. a. Æ. Exploring Chemistry with Electronic Structure Methods. 3rd ed edn, (Gaussian, Inc., 2015).
25 Bandaranayake, K. P., Sivakumar, V., Wang, R. & Hastings, G. Modeling the A1 binding site in photosystem: I. Density functional theory for the calculation of "anion− neutral" FTIR difference spectra of phylloquinone. Vibrational Spectroscopy 42, 78-87 (2006).

Citation:
Neva Agarwala, Daniel Ranke, Leyla Rohani, and Gary Hastings (2019) Calculated and Experimental Infrared Spectra of Substituted Naphthoquinones, *Frontiers in Science, Technology, Engineering and Mathematics*, **Volume 3**, Issue 2, 71-80